

HydroDeep – A Knowledge Guided Deep Neural Network for Geo-Spatiotemporal Data Analysis

Aishwarya Sarkar¹, Jien Zhang², Chaoqun Lu², Ali Jannesari¹

¹Department of Computer Science, Iowa State University

²Department of Ecology, Evolution, and Organismal Biology, Iowa State University
{asarkar1, jienz, clu, jannesar}@iastate.edu

Abstract

Floods are one of the major climate-related disasters, leading to substantial economic loss and social safety issue. However, the confidence in predicting changes in fluvial floods remains low due to limited evidence and complex causes of regional climate change. The recent development in machine learning techniques has the potential to improve traditional hydrological models by using monitoring data. Although Recurrent Neural Networks (RNN) perform remarkably with multivariate time series data, these models are blinded to the underlying mechanisms represented in a process-based model for flood prediction. While both process-based models and deep learning networks have their strength, understanding the fundamental mechanisms intrinsic to geospatiotemporal information is crucial to improve the prediction accuracy of flood occurrence. This paper demonstrates a neural network architecture (HydroDeep) that couples a process-based hydro-ecological model with a combination of Deep Convolutional Neural Network (CNN) and Long Short-Term Memory (LSTM) Network to build a hybrid baseline model. HydroDeep outperforms the performance of both the independent networks by 4.8% and 31.8% respectively in Nash–Sutcliffe efficiency. A trained HydroDeep can transfer its knowledge and can learn the Geo-spatiotemporal features of any new region in minimal training iterations.

1 Introduction

Flood events are the most frequent type of natural disasters worldwide. The recent surge in population growth and rapid urbanization makes it extremely essential to tackle this problem. Every year, farmlands and urban infrastructures go through significant and sometimes irreparable damages due to flash floods. Risk prediction and risk mitigation are two components of risk management. Prediction of flash floods is necessary to delegate proper risk management resources to minimize associated damages.

The urban population will reach 6 billion by 2030 (U.N., 2006). Urbanization in congested smaller areas with a concentrated population, wealth, and infrastructure invariably increases the flood risk. Cities on coastal or river deltas are at high risk due to large-scale runoff changes, potentially raising sea level. Major U.N. studies reveal that the recent extent of climate change is endangering the future of life on this planet. The increased recurrence of flood events around the world is partially accounted for the climate change-driven

increase of extreme precipitation (CHANGE et al. 2007; Bernstein et al. 2008). In 2019, about a quarter-million acres of fertile farmland was underwater for four months in the Mississippi Delta region. This uncalled-for event was devastating to the farmers hurting the local economy of the region. In "The Great Flood of 2019: A Complete Picture of a Slow-Motion Disaster," New York Times reports with an interactive composite map showing all the Midwest and Southern regions in the U.S. inundated at some point for the first half of the year. They claim that the event affected nearly 14 million people. The data used by them to measure spring floods shows an interconnected catastrophe along the Michigan, Mississippi, and Arkansas Rivers that drain more than 40% of the United States' landmass. More than 400 counties from at least 11 states had to sought federal disaster funds to cover their damages. (Sarah Almukhtar and Williams September 11, 2019)

Planning for effective risk management of flood can only be done when the extent of its nature is predicted. Huong and Pathirana, in their study of a third-world city points out the four major challenges that can lead to a combined impact resulting in flood - (i) climate change-driven sea-level rise, (ii) climate change-driven increase of river runoff, (iii) increase of urbanization that leads to increased imperviousness in surface and sub-surface water flow, (iv) enhancement of extreme rainfall due to urban growth-driven microclimatic change (urban heat islands (Huong and Pathirana 2013)). Taking preventive measures towards each of these challenges will give us a fair chance at avoiding the impacts of flood.

In recent decades, prevalent global warming is also accelerating the global water cycle resulting in enhanced flood frequency. Cyclones and hurricanes appear to have an increase in frequency and intensity. In hydrological sciences, modeling of rainfall-runoff in an attempt to predict discharge as a function of precipitation using approaches of regression date back 170 years (Beven 2011; Mulvaney 1851). Researchers have incorporated more profound concepts of physical properties of the catchments, boundary conditions, and spatial variability into mathematical model formulations after years of progressive development. Due to a large degree of uncertainty with the current approaches, the quantitative estimation of climate change impact on extreme rainfall events is currently an active research area.

This work's main social impact is to propose a novel neural network architecture - HydroDeep based on a combination of Convolutional Neural Networks (CNN) and Long Short-Term Memory Networks (LSTM) to learn the Geospatiotemporal features that lead to an event of a flood. In our experiment which we will discuss shortly, HydroDeep outperformed the Nash–Sutcliffe efficiency of CNN by 4.8% and LSTM by 31.8%. Additionally, we propose a novel approach of transferring the knowledge of the trained HydroDeep model to any unknown region with sparse dataset availability. This method reduces extensive training time and makes it computationally cheaper than the state of the art deep learning techniques that are currently used extensively to predict a flood.

Our contributions are as follows:

- HydroDeep - A hydrological knowledge powered deep neural network to forecast flood.
- The ability to transfer knowledge to diverse regions to reduce extensive training time and large-scale dataset dependency.
- A novel approach to utilize the closest precipitation measurements to the prediction day.

2 Background and Related Works

Since the year 2018, the average number of publications in the applications of deep learning techniques increased steadily in an exponential function (Sit et al. 2020). Custom AI solutions developed by the computer science community holds a promising potential to help the hydrology community. One of the preliminary researches were performed in the 1990s, where Artificial Neural Networks (ANN) were used for rainfall-runoff prediction (Daniell 1991). However, the disadvantage of using ANN in time-series analysis is that they fail to retain the sequential order of the inputs. Here, Recurrent Neural Networks (RNN) come to rescue. The main idea behind RNNs is to use sequential information in time-series data. A special kind of RNN, the Long Short-Term Memory Networks (LSTM) can learn long-term temporal dependencies and outperform ANN in rainfall-runoff simulation (Hu et al. 2018). Several recent studies have also coupled a process-based model with deep learning networks and claims that the inclusion of hydrological model prediction is useful to real-time reservoir operation (Yang et al. 2019). Along with LSTM, Gated Recurrent Units (GRU) are used in some studies to model rainfall-runoff (Sit and Demir 2019). The implementation of a hybrid network of LSTM-seq2seq with GRUs outperformed the individual state of the art performance in the studies of the Clear Creek Watershed in Iowa (Xiang and Demir 2020). Along with recurrent neural networks, 1D Convolutional Neural Networks also show promising performance in rainfall-runoff modeling where two parallel convolution filters process separate time series that allows faster processing of data (Van et al. 2020). A Long-term Recurrent Convolutional Network (LRCN) model, as initially named is a combination of CNN and LSTM that has been recently developed to generate a textual description of images in Computer Vision (Donahue et al. 2015). This architecture has also been used in

Speech Recognition and Natural Language Processing problems where the convolutional layers are used for extracting features for the LSTMs (Vinyals et al. 2015). Results from a deep neural network model (APNet) based on CNN and LSTM outperforms all the traditional deep learning models commonly used in time-series analysis.(Huang and Kuo 2018).

3 Approach

Image classification problems widely use 2D and 3D Convolutional Neural Networks (CNN). Its ability to learn features also stays the same in one-dimensional sequences of data. Recent researches have shown that using CNNs for time series classification has several significant advantages over other methods. Being highly noise-resistant models, they can extract very informative and in-depth features independent of time. One-dimensional CNN is also widely used in Natural Language Processing problems. When applied to the one-dimensional time series data, the convolutional layers map the internal features of the sequence. Our neural network architecture combines a series connection of Convolutional Neural Network (CNN) with Long Short-Term Memory (LSTM) for multivariate time series prediction. This integration improves the prediction performance of individual CNN and LSTM by making the most of both the spatial and temporal dependencies. The upper convolutional layers extract spatial features between the input variables, which consists of daily precipitation measurements and pixel-based runoff estimates from a process-based hydro-ecological model (DLEM) and pass the results to the next layer. These layers are combined with LSTMs to support sequence prediction. The convolutional operation reduces the number of parameters making the CNN-LSTM network deeper.

3.1 The Process-based Model

The Dynamic Land Ecosystem Model (DLEM) that we use in this work is a process-based (PB) hydro-ecological model that is designed to mimic the plant physiological, biogeochemical and hydrological processes in the plant-soil-water-river continuum (Liu et al. 2013; Lu and Tian 2013; Yang et al. 2015). In DLEM, river network and in-stream processes are incorporated into a terrestrial modeling scheme, and the design of grid-to-grid connection allows us to track major features of the DLEM model including within-grid heterogeneity, grid-to-grid connection, and land-aquatic linkage. The water movement from land to aquatic systems is modeled at a daily time step. In DLEM, each grid cell is a cohort of multiple land cover types, rivers, and lakes with their area percentage prescribed by land-use history data (Lu et al. 2020). The DLEM has been extensively validated against measurements from LTER, NEON, Ameri Flux, USDA crop yield survey, and USGS gauge monitoring, and widely used to quantify the spatiotemporal variations in the pool and fluxes of water-C-N at the site-and regional scales (Liu et al. 2013; Lu and Tian 2013; Yang et al. 2015; Yu et al. 2019; Lu et al. 2019; Tian et al. 2011; Zhang et al. 2018; Feng et al. 2015; Tian et al. 2012; Liu et al. 2008;

Lu et al. 2012). The preliminary results from DLEM show that the variations of daily river discharge are very close to the USGS observed river discharge at the outlet of the Mississippi and Atchafalaya river basin (MARB) over the years (Figure 1) (Lu et al. 2020). However, the DLEM capability in capturing extremely high daily river discharge is still limited (Figure 1). Therefore, combining the strength of the ML approach in capturing the “outliers” with the PB model will largely increase the model’s capability of predicting flooding.

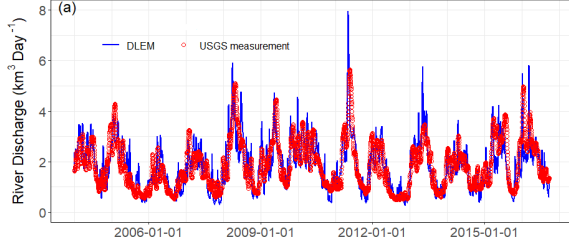


Figure 1: Comparison of DLEM-modeled and USGS-monitored daily river discharge from the Mississippi and Atchafalaya river basin (MARB). The daily river discharge is from April 1, 2004 to September 28, 2016. The USGS river discharge was calculated based on the daily river discharge measurements at the Melville gauge station (station ID 07381495) measuring the discharge of Atchafalaya River and at St. Francisville gauge station (07373420) measuring the discharge of the Mississippi River.

3.2 HydroDeep

Problem Statement If $g_i^0 = \{g_1, g_2, \dots, g_n\}$ is the spatial grid vector where n is the number of grids covering a region having spatial coordinates $c_i^0 = \{x_1, y_1\}, \{x_2, y_2\}, \dots, \{x_n, y_n\}$, the distance to these coordinates from the nearest river or water source is $d_i^0 = \{d_1, d_2, \dots, d_n\}$. The grids have precipitation measurements as one of the input vectors $p_i^0 = \{p_1, p_2, \dots, p_n\}$ which is mapped to its corresponding grid-based DLEM-runoff estimates, $r_i^0 = \{r_1, r_2, \dots, r_n\}$. The input vectors are labelled with daily river discharge observations D_i^0 . (Equation 1)

$$Matrix_i = \{d_i, p_i, r_i, D_i\} \quad (1)$$

From a multivariate time-series point of view, we can define the problem more formally. Given an input sequence of time-series signals $X = (x_1, x_2, \dots, x_T)$ with $x_t \in \mathbb{R}^n$, where the variable dimension is n , we want to predict the corresponding target outputs $Y = (y_1, y_2, \dots, y_h)$. The aim is to obtain a non-linear mapping between X and Y as shown in Equation 2.

$$(y_1, y_2, \dots, y_h) = f(x_1, x_2, \dots, x_T) \quad (2)$$

Input Data The precipitation measurement of the target prediction day plays a catalyst for a flood event. A continuous drought for a stretch of days can be followed by a hurricane which may lead to flood overnight. Hence it only

seemed crucial to include the target day’s input drivers into the network. HydroDeep, as we named our model takes two inputs at different stages of the network to accommodate the prediction day’s inputs and then the model is trained as an end-to-end network. The first input comes from the precipitation and DLEM-runoff estimates from $(t - lag)$ to $(t - 1)$ days. The term “lag” refers to the number of days in the past whose input data is required to train the prediction model. t is referred to as the prediction day. The second input has the independent variables (precipitation and DLEM-runoff estimates) of the prediction day t , that are concatenated with the sequenced temporal data halfway through the network.

Workflow Since watersheds vary in area, each watershed has different number of grids covering its area. To make our model more adaptive, HydroDeep has an initial input layer that is customizable to different input shapes. The input layer gets the precipitation and DLEM-runoff from $t - lag$ through $t - 1$ days as the first input (Figure 2). A couple of convolutional layers are then applied to the inputs followed by a max-pooling layer. The pooling layer combines the output of a cluster of neuron from the convolution layers into a single neuron into the next layer. This reduces the number of parameters at hand along with the computation cost of the network. Then we have four LSTM layers with dropouts applied to the last layer. The dropout technique is used to regularize the network and avoid overfitting. The LSTM layer utilizes its memory units to preserve long-term memory that updates previous hidden state. The output values from the convolution layers are passed into the gate units. Each LSTM layers have three gate units - input, output and forget gate. These three gate units determine the state of each individual memory cell through multiplication operations. The memory cells updates their states as each gate unit gets activated. The hidden state of the LSTM cells is h_t at every time-step t .

$$f_t = \sigma(W_f \cdot [h_{t-1}, x_t] + b_f) \quad (3)$$

$$i_t = \sigma(W_i \cdot [h_{t-1}, x_t] + b_i) \quad (4)$$

$$o_t = \sigma(W_o \cdot [h_{t-1}, x_t] + b_o) \quad (5)$$

Equation 3, 4 and 5 show the respective mathematical operations of the forget gate, the input gate and the output gate. The notations f , i and o show the output of the said operations. σ is the non-linear *sigmoid* activation function which is used at the gates that only allows values between $[0, 1]$. The weight matrix of each unit gate is W and their bias vector is b . The cell states and the hidden states are formulated from the forget, the input and the output gate and are shown in Equation 6 and 7 respectively. The cell state defined as C_t uses *tanh* to restrict its values between -1 and 1. This is multiplied by the output of the sigmoid gate o_t .

$$C_t = f_t * C_{t-1} + i_t * \tanh(W_C \cdot [h_{t-1}, x_t] + b_C) \quad (6)$$

$$h_t = o_t * \tanh(C_t) \quad (7)$$

At this stage the second input layer is fed into the network through a concatenation layer that concatenates the output of previous LSTM layers with the second input. The second input as part of the learned temporal sequence now goes

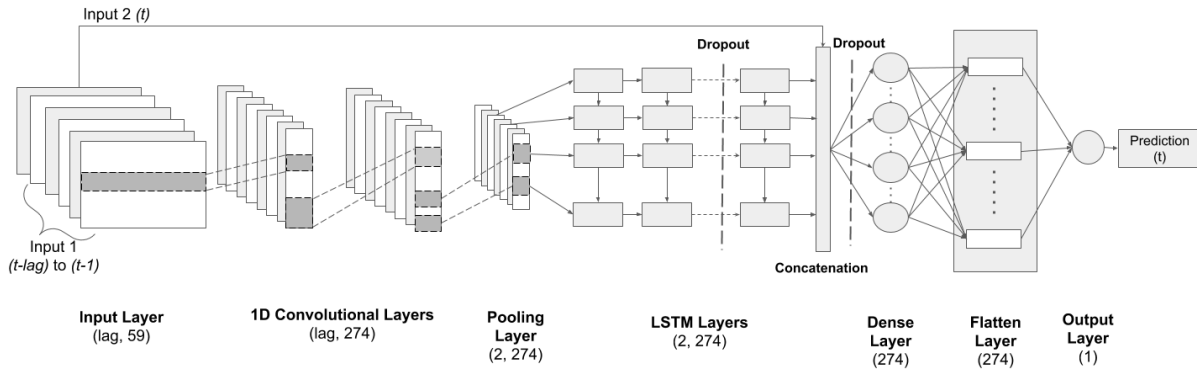


Figure 2: HydroDeep Network Architecture

through one dense layer to get mapped with the prediction day t 's dependent variable. The dense layer is then followed by a Dropout layer for regularization. The final layer is the output layer which predicts the river discharge measurement at day t .

3.3 Transfer Learning

An extension to our HydroDeep model is its ability to transfer its knowledge to other watersheds which reduces the training duration required to train on new dataset. By definition, transfer learning consists of a domain D and a task T where the domain D is the marginal probability distribution $P(X)$ over a feature space $X = \{x_1, x_2, \dots, x_n\}$. Given a domain $D = \{X, P(X)\}$, a task T consists of a conditional probability distribution $P(Y|X)$ over a label space Y . The conditional probability distribution is usually learned from the pairs $\{x_i, y_i\}$ in the training samples where $x_i \in X$ and $y_i \in Y$. Suppose there is a source domain D_s with a source task T_s and a target domain D_t with a target task T_t , through transfer learning we try to learn the target conditional probability distribution $P(Y_t|X_t)$ in target domain D_t , from the knowledge learned from D_s and T_t .

For our experiment, we chose Thompson Fork Grand River basin at David City (watershed 13) as our source domain and transferred its knowledge to a target domain - West Nodaway River near Shambaugh (watershed 14) (Jones et al. 2018). We evaluated three known approaches of transfer learning for our work and we present the detailed findings in the results section.

4 Experimental Design

4.1 Dataset

We use the daily discharge measurements for Iowa Streams obtained from U.S. Geological Survey (USGS) as our field observations (Jones et al. 2018). The dataset has daily measurements covering 23 watersheds within Iowa (Figure 3). The red triangles in the figure are the outlets where the river discharge measurements were observed. Daily precipitation at a 5-arc-min resolution used in this study were generated from high-resolution gridded meteorological data products from station observations by the Climatic Research Unit

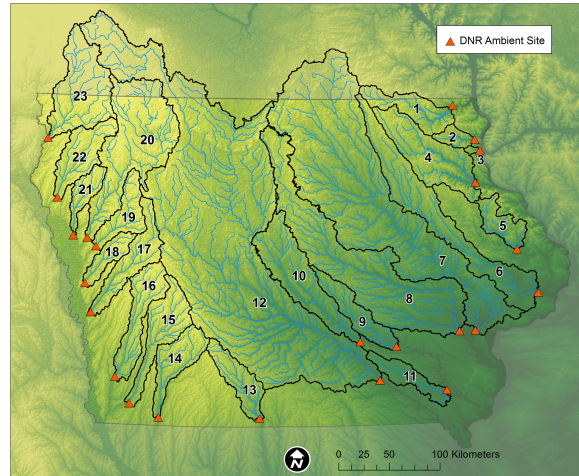


Figure 3: Iowa Stream Sites and observation regions. The daily river discharge observations are recorded at each red triangle. The numbers correspond to watersheds. (Jones et al. 2018)

(CRU) of the University of East Anglia (Mitchell and Jones 2005) and North America Regional Reanalysis (NARR) dataset from a combination of modeled and observed data (Mesinger et al. 2006). We also use DLEM-simulated surface and subsurface runoff as our environmental input driver (Lu et al. 2020). The DLEM simulation forced by climate, management, and environmental drivers was used to represent our “best estimate” of land-to-aquatic surface and subsurface runoff across the watershed.

4.2 Distance as a spatial weight

In addition, the extent to which each input grid contributes to the river discharge depends extensively on the distance to the nearest river. We used these distances as weights to our input precipitation and runoff data. Considering there are m number of grids in a watershed, each grid is denoted by g_m^n for n number of days. We take each pixel's correspond-

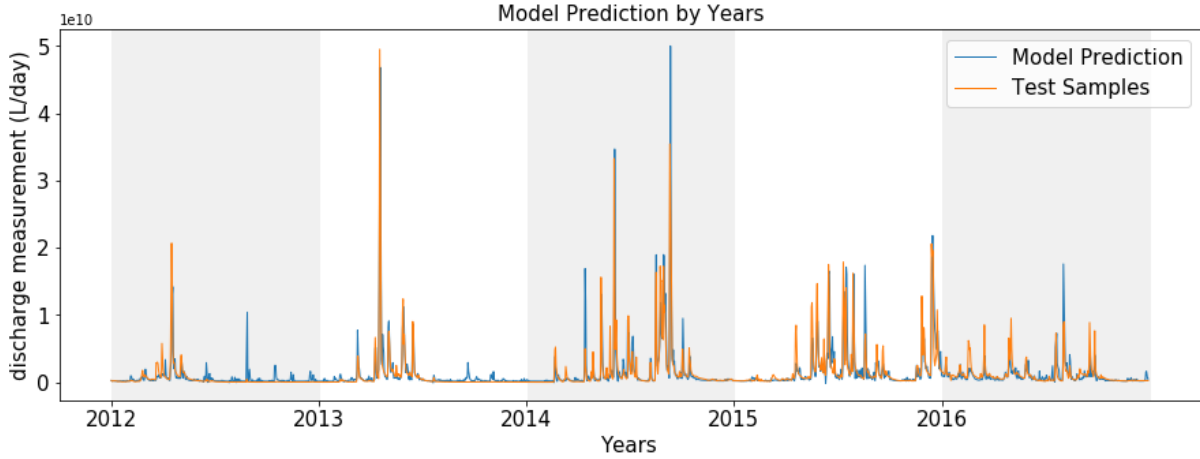


Figure 4: The HydroDeep-predicted daily river discharge is plotted against river gauge measurements from Jan 1, 2012 to Dec 31, 2016.

ing spatial coordinates (x_m^n, y_m^n) to calculate its distance d_m^n from the nearest local river. We take the dot product of the the physical distances from the nearest water source with the grid-based inputs to drive our network. We use a series-to-supervised function to transform the raw data into the form suitable for supervised learning. The data are split into training samples where for every sample, we are looking back at z days of historical data. Hence, to forecast a discharge measurement label at a specific day t , the input features from $(t - lag)$ day to t day is considered where lag is the time-step or lookback value.

4.3 Model Parameter Settings

The raw spatially weighted precipitation data undergoes normalization to ensure all the data is unified to $[0, 1]$. After transforming the input dataset into samples along with its lookback features, the whole dataset of samples is split into a training set and a validation set in the ratio of 7:3, respectively. The model runs for a maximum of 300 epochs set manually with a batch size of 32 in each epoch. The problem of over-training is taken care of with the implementation of early stopping to ensure that the model keeps monitoring the loss value with the patience of 50 epochs. It is further optimized by Adam optimizer. After the training is complete, the values are inverse-transformed, and the model prediction is plotted against ground-truth values (Figure 4).

5 Results

5.1 Evaluation Metrics

The model is evaluated with Root Mean Square Error (RMSE) and Nash–Sutcliffe efficiency (NSE) (Nash and Sutcliffe 1970). These metrics calculate the correlation coefficient of the observed and the model simulated discharge. In Equation 8, P_i is the predicted value and O_i is the observed value over the number of samples n . In Equation 9, Q_o is the mean of observed discharge, Q_m is the predicted discharge whereas Q_o^t is the observed discharge

at time t .

$$RMSE = \sqrt{\frac{1}{n} \sum_{i=1}^n (P_i - O_i)^2} \quad (8)$$

$$NSE = 1 - \frac{\sum_{t=1}^T (Q_m^t - Q_o^t)^2}{\sum_{t=1}^T (Q_o^t - \bar{Q}_o)^2} \quad (9)$$

The NSE is equivalent to the coefficient of determination R^2 and is one of the most commonly used metrics by hydrologists to evaluate their models' performance.

5.2 Hyperparameter Tuning

One of the main hyperparameters that our model was sensitive to is the lookback (lag) parameter. The LSTM tries to look back at the historical data, and that knowledge is used to predict the event of the target day. While the network is be-

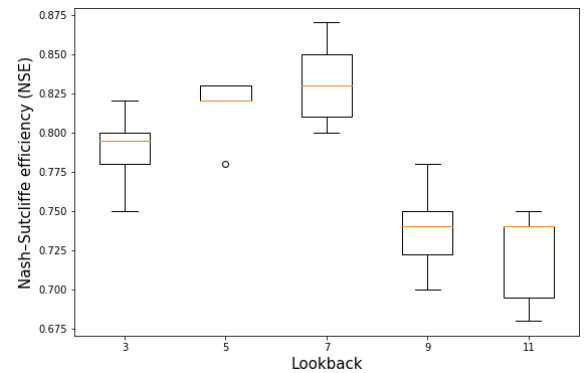


Figure 5: NSE of different model runs on watershed 13 with various lookback values in HydroDeep.

ing trained, the lookback window slides over all the training samples with a step value of 1 day per iteration. Our network

Models	RMSE (km^3)	NSE
HydroDeep	1085.9	0.87
Convolutional Neural Network (CNN)	1206.3	0.83
Bi-directional Long Short-Term Memory Network	1507.4	0.75
Gated Recurrent Unit (GRU)	1561.9	0.73
Long Short-Term Memory Network (LSTM)	1768.2	0.66

Table 1: Comparisons with other benchmark neural network architectures

also uses target day t 's input parameters to sense any immediate upsurge or down surge in precipitation on the target t day that might cause a spike in river discharge measurements resulting in the event of a flood. Figure 5 shows our experiment with different short term lookback values and how it affects the Nash–Sutcliffe efficiency of HydroDeep.

We performed 10 model runs and the result shows that learning from 11 days of historical data had the lowest median NSE. So the increase of performance with the increase of number of lookback days was not observed at least for watershed 13. We continued the rest of our work with a lookback of 7 days because of its higher median NSE throughout. We further optimized the hyperparameters and evaluated the performance on our test dataset. The test split contains the model predicted river discharge measurements from the year 2012 to the year 2016. We compared these values against the ground truth observations. The results are shown in Figure 4. Additionally, we compare the performance of HydroDeep in predicting river discharge measurements of watershed 13 with other benchmark architectures that are used in similar applications (Table 1). We will discuss about this in the next section.

5.3 Transferring Knowledge

We have experimented with three transfer learning approaches - freezing all source model layers, fine-tuning source model layers, and freezing some of the layers while letting the rest fine-tune for target domain.

Freezing all model layers The first approach is to freeze all the network layers from the source model without enabling them to fine-tune on new data.

Fine-Tuning model layers The second approach our model extension followed was to allow new data to fine-tune all its layers.

Freezing and fine-tuning on new watershed We froze the top convolutional layers, and let the recurrent layers fine-tune on the new temporal dependencies specific to the concerned region. This proved to be the best approach in our application area. In Figure 6, Transferred HydroDeep refers to a scenario where HydroDeep was fully trained on source watershed 13. The trained model was then saved and used in predicting unknown samples from adjacent watershed 14. We let the trained model to fine-tune on the new watershed for a smaller number of iterations. The term HydroDeep in the figure refers to a previously untrained HydroDeep network which is then trained from scratch for 20 iterations on watershed 14. The figure shows a 20 day window where a

spike in river discharge measurement is observed in watershed 14 in the year 2016. We ran 20 iterations of HydroDeep and Transferred HydroDeep to predict the spike.

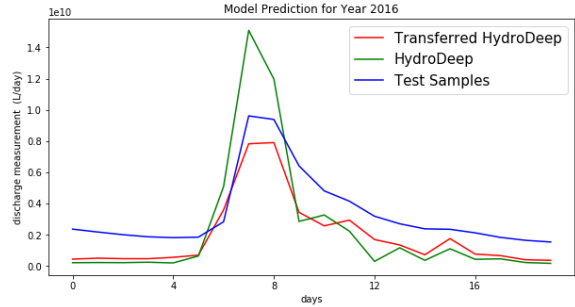


Figure 6: A 20 day window of watershed 14 from the year 2013 where a spike had occurred in the river discharge measurement.

6 Discussion

This section will discuss how HydroDeep outperforms all the state of the art networks with the knowledge acquired from the process-based model. CNN-LSTM networks are more capable of capturing short-term and long-term patterns compared to the baseline models. In predicting unknown test samples from one of the smaller watersheds (watershed 13), HydroDeep captured the peaks and troughs with 0.63 NSE. This work's main motive is to have a trained deep neural network driven by process-based knowledge from hydrological models to improve the prediction accuracy for the event of a flood or the spikes in the temporal trend of river discharge measurements. The NSE on the test samples is observed to be low. This is because the model can predict the spikes correctly but predicts the volume of water during the flood events with an RMSE of 1085.9 cubic kilometers in volume. In Figure 7, we present a window of 100 days from the watershed 13, which shows how HydroDeep has predicted one of the spikes in river drainage water that occurred in the year 2013. We believe HydroDeep's prediction of the volume of water during a flood can be improved with more training on diverse watersheds.

In transferring the knowledge of HydroDeep to other watersheds, we had designed three experimental setups to explore the abilities of HydroDeep in performing in a never seen watershed. Watersheds vary in characteristics as the soil property and land usage change from region to region. Due to the variance in physical features, the hydrological mech-

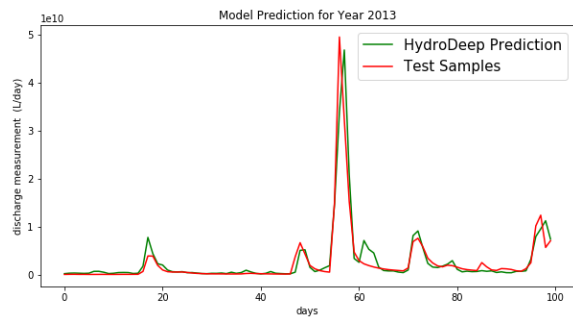


Figure 7: A closer look at a 100 days window of watershed 13 in the year 2013.

anisms change. In our first approach, we had tried to freeze all the layers of HydroDeep and tested its performance on an adjacent watershed (watershed 14). We observed that even though the source domain and the target domain were closer to each other, the training of the network on the features of watershed 13 alone was not enough to predict the spatiotemporal features of watershed 14. The primary purpose of transferring knowledge to other regions is to learn the features of a watershed considerably well in shorter iterations. In our second approach, we let all the layers of HydroDeep fine-tune on the spatial and temporal features of watershed 14. While HydroDeep started to learn the new features of watershed 14, it lost previously learned fundamental features of watersheds. Due to the smaller number of iterations, it neither could learn the features of watershed 14 nor could remember the parameters from its source domain (watershed 13).

We resolved this problem by our third approach. In this approach, we let a few HydroDeep’s convolutional layers retain their spatial knowledge from the source domain (watershed 13) and let the other layers fine-tune on the target domain (watershed 14). Figure 6 verifies that Transferred HydroDeep can model a particular observed spike’s temporal trend in much smaller training iterations by fine-tuning its learned parameters on the new features rather than starting to learn from scratch.

7 Conclusion and Future Work

This paper illustrates a new approach to analyze Geospatiotemporal information. The utilization of process-based knowledge and spatial features has proved to drive neural networks to be more efficient in predicting flood events. This is due to the fact that different spatiotemporal problems have distinctive sets of dynamic systems driven by their unique physical properties. A combination of Deep Convolutional Neural Networks to learn the Geospatial features drove HydroDeep to better performance. These learned spatial features steered the Long Short-Term Memory layers to discover the temporal features of the watersheds. Furthermore, the Transferred HydroDeep proved to be more useful in learning the Geo-spatiotemporal features of a new watershed in minimal training iterations, which lowers the computational cost. This end-to-end network will prove highly

beneficial to society in predicting the events of flood and mitigate socio-economical damages.

We have currently worked with Thompson Fork Grand River basin at David City (watershed 13) and West Nodaway River near Shambaugh (watershed 14) in Iowa, and HydroDeep performed better than all the state of the art networks. In the future, we would like to extend the training of our model to larger watersheds having more diverse characteristics that will enable our network to work better in transferring knowledge to any new watershed. Additionally, we also want to expand this work with Generative Adversarial Networks to create artificial training data for HydroDeep. This future work will improve HydroDeep’s performance further as a transferrable source model that can be fine-tuned for other watersheds with sparse data availability.

References

- Bernstein, L.; Bosch, P.; Canziani, O.; Chen, Z.; Christ, R.; Davidson, O.; Hare, W.; Huq, S.; Karoly, D.; Kattsov, V.; et al. 2008. *Climate change 2007: Synthesis report: An assessment of the intergovernmental panel on climate change*. IPCC.
- Beven, K. J. 2011. *Rainfall-runoff modelling: the primer*. John Wiley & Sons.
- CHANGE, O. C.; et al. 2007. Intergovernmental panel on climate change. *World Meteorological Organization*.
- Daniell, T. M. 1991. Neural networks. Applications in hydrology and water resources engineering. *Proceedings of the International Hydrology and Water Resource Symposium 3*: 797–802. doi:10.1061/(ASCE)1084-0699(2000)5:2(124).
- Donahue, J.; Anne Hendricks, L.; Guadarrama, S.; Rohrbach, M.; Venugopalan, S.; Saenko, K.; and Darrell, T. 2015. Long-term recurrent convolutional networks for visual recognition and description. In *Proceedings of the IEEE conference on computer vision and pattern recognition*, 2625–2634.
- Feng, Y.; Friedrichs, M. A.; Wilkin, J.; Tian, H.; Yang, Q.; Hofmann, E. E.; Wiggert, J. D.; and Hood, R. R. 2015. Chesapeake Bay nitrogen fluxes derived from a land-estuarine ocean biogeochemical modeling system: Model description, evaluation, and nitrogen budgets. *Journal of Geophysical Research: Biogeosciences* 120(8): 1666–1695.
- Hu, C.; Wu, Q.; Li, H.; Jian, S.; Li, N.; and Lou, Z. 2018. Deep Learning with a Long Short-Term Memory Networks Approach for Rainfall-Runoff Simulation. *Water* 10(11): 1543. ISSN 2073-4441. doi:10.3390/w10111543. URL <http://dx.doi.org/10.3390/w10111543>.
- Huang, C.-J.; and Kuo, P.-H. 2018. A Deep CNN-LSTM Model for Particulate Matter (PM_{2.5}) Forecasting in Smart Cities. *Sensors* 18(7): 2220. ISSN 1424-8220. doi:10.3390/s18072220. URL <http://dx.doi.org/10.3390/s18072220>.
- Huong, H. T. L.; and Pathirana, A. 2013. Urbanization and climate change impacts on future urban flooding in Can Tho city, Vietnam. *Hydrology and Earth System Sciences* 17(1): 379.
- Jones, C. S.; Nielsen, J. K.; Schilling, K. E.; and Weber, L. J. 2018. Iowa stream nitrate and the Gulf of Mexico. *PLoS one* 13(4): e0195930.
- Liu, M.; Tian, H.; Chen, G.; Ren, W.; Zhang, C.; and Liu, J. 2008. Effects of Land-Use and Land-Cover Change on

- Evapotranspiration and Water Yield in China During 1900–2000. *JAWRA Journal of the American Water Resources Association* 44(5): 1193–1207.
- Liu, M.; Tian, H.; Yang, Q.; Yang, J.; Song, X.; Lohrenz, S. E.; and Cai, W.-J. 2013. Long-term trends in evapotranspiration and runoff over the drainage basins of the Gulf of Mexico during 1901–2008. *Water Resources Research* 49(4): 1988–2012.
- Lu, C.; and Tian, H. 2013. Net greenhouse gas balance in response to nitrogen enrichment: perspectives from a coupled biogeochemical model. *Global change biology* 19(2): 571–588.
- Lu, C.; Tian, H.; Liu, M.; Ren, W.; Xu, X.; Chen, G.; and Zhang, C. 2012. Effect of nitrogen deposition on China's terrestrial carbon uptake in the context of multifactor environmental changes. *Ecological applications* 22(1): 53–75.
- Lu, C.; Zhang, J.; Cao, P.; and Hatfield, J. L. 2019. Are we getting better in using nitrogen?: Variations in nitrogen use efficiency of two cereal crops across the United States. *Earth's Future* 7(8): 939–952.
- Lu, C.; Zhang, J.; Tian, H.; Crumpton, W.; Helmers, M.; Cai, W.; Hopkinson, C.; and Lohrenz, S. 2020. Increased extreme precipitation challenges nitrogen load reduction to the Gulf of Mexico. *Communications Earth & Environment* Accepted. doi:DOI:10.1038/s43247-020-00020-7.
- Mesinger, F.; DiMego, G.; Kalnay, E.; Mitchell, K.; Shafran, P. C.; Ebisuzaki, W.; Jović, D.; Woollen, J.; Rogers, E.; Berbery, E. H.; Ek, M. B.; Fan, Y.; Grumbine, R.; Higgins, W.; Li, H.; Lin, Y.; Manikin, G.; Parrish, D.; and Shi, W. 2006. North American Regional Reanalysis. *Bulletin of the American Meteorological Society* 87(3): 343–360. ISSN 0003-0007. doi:10.1175/BAMS-87-3-343. URL <https://doi.org/10.1175/BAMS-87-3-343>.
- Mitchell, T. D.; and Jones, P. D. 2005. An improved method of constructing a database of monthly climate observations and associated high-resolution grids. *International Journal of Climatology* 25(6): 693–712. doi:10.1002/joc.1181. URL <https://rmets.onlinelibrary.wiley.com/doi/abs/10.1002/joc.1181>.
- Mulvaney, T. J. 1851. On the use of self-registering rain and flood gauges in making observations of the relations of rainfall and flood discharges in a given catchment. *Proceedings of the institution of Civil Engineers of Ireland* 4: 19–31.
- Nash, J. E.; and Sutcliffe, J. V. 1970. River flow forecasting through conceptual models part I—A discussion of principles. *Journal of hydrology* 10(3): 282–290.
- Sarah Almkhatar, Blacki Migliozi, J. S.; and Williams, J. September 11, 2019. The Great Flood of 2019: A Complete Picture of a Slow-Motion Disaster. *The New York Times*.
- Sit, M.; and Demir, I. 2019. Decentralized flood forecasting using deep neural networks. *arXiv preprint arXiv:1902.02308*.
- Sit, M.; Demiray, B. Z.; Xiang, Z.; Ewing, G. J.; Sermet, Y.; and Demir, I. 2020. A comprehensive review of deep learning applications in hydrology and water resources. *Water Science and Technology*.
- Tian, H.; Chen, G.; Zhang, C.; Liu, M.; Sun, G.; Chappelka, A.; Ren, W.; Xu, X.; Lu, C.; Pan, S.; et al. 2012. Century-scale responses of ecosystem carbon storage and flux to multiple environmental changes in the southern United States. *Ecosystems* 15(4): 674–694.
- Tian, H.; Xu, X.; Lu, C.; Liu, M.; Ren, W.; Chen, G.; Melillo, J.; and Liu, J. 2011. Net exchanges of CO₂, CH₄, and N₂O between China's terrestrial ecosystems and the atmosphere and their contributions to global climate warming. *Journal of Geophysical Research: Biogeosciences* 116(G2).
- Van, S. P.; Le, H. M.; Thanh, D. V.; Dang, T. D.; Loc, H. H.; and Anh, D. T. 2020. Deep learning convolutional neural network in rainfall–runoff modelling. *Journal of Hydroinformatics* 22(3): 541–561.
- Vinyals, O.; Toshev, A.; Bengio, S.; and Erhan, D. 2015. Show and tell: A neural image caption generator. In *Proceedings of the IEEE conference on computer vision and pattern recognition*, 3156–3164.
- Xiang, Z.; and Demir, I. 2020. Distributed Long-term Hourly Runoff Predictions Using Deep Learning—A Case Study for State of Iowa.
- Yang, Q.; Tian, H.; Friedrichs, M. A.; Hopkinson, C. S.; Lu, C.; and Najjar, R. G. 2015. Increased nitrogen export from eastern North America to the Atlantic Ocean due to climatic and anthropogenic changes during 1901–2008. *Journal of Geophysical Research: Biogeosciences* 120(6): 1046–1068.
- Yang, S.; Yang, D.; Chen, J.; and Zhao, B. 2019. Real-time reservoir operation using recurrent neural networks and inflow forecast from a distributed hydrological model. *Journal of Hydrology* 579: 124229.
- Yu, Z.; Lu, C.; Tian, H.; and Canadell, J. G. 2019. Largely underestimated carbon emission from land use and land cover change in the conterminous United States. *Global change biology* 25(11): 3741–3752.
- Zhang, J.; Tian, H.; Yang, J.; and Pan, S. 2018. Improving representation of crop growth and yield in the Dynamic Land Ecosystem Model and its application to China. *Journal of Advances in Modeling Earth Systems* 10(7): 1680–1707.